Article

Thermal Safety Evaluation of Silane Polymer Compounds as Electrolyte Additives for Silicon-Based Anode Lithium-Ion Batteries

Chuan-Zhu Zhang [1], Lin-Jie Xie [1], Yan Tang [1], You Li [2], Jun-Cheng Jiang [1,*] and An-Chi Huang [1,*]

[1] School of Safety Science and Engineering, Changzhou University, Changzhou 213164, China
[2] School of Overseas Education, Changzhou University, Changzhou 213164, China
* Correspondence: jiangjc@cczu.edu.cn (J.-C.J.); huangac@cczu.edu.cn (A.-C.H.)

Abstract: The capacity fading and thermal safety issues caused by the volume effect of Si-based anodes and unstable solid electrolyte interphase (SEI) films during long-term cycling limit its large-scale application. In this study, silane polymer compound (2-cyanoethyl) triethoxysilane (TCN) was selected as an electrolyte additive to improve the reversibility and thermal safety of Si-based anode lithium-ion batteries (LIBs). TCN prevented the thermal interaction between the vitiated anode and electrolyte, and the onset temperature of the thermal reaction increased from 122.22 to 127.07 °C, as demonstrated by the results of thermogravimetric analysis and differential scanning calorimetry. The thermal stability of lithiated anodes containing various electrolytes was then assessed using a range of thermo-kinetic models. The results revealed that the activation energy of Si-based lithiated anodes increased from 68.46 to 91.32 kJ/mol, while the thermal hazard greatly decreased. Additionally, the electrochemical test and characterization results showed that TCN helped generate a stable SEI coating with more Li_2CO_3 components, which improved the cells' cycle stability. This study provides a new reference for the growth of LIBs with high security and energy density.

Keywords: silicon-based anode; thermogravimetric analyzer; thermokinetic model; electrolyte additive; lithium-ion battery

1. Introduction

In recent years, the rapid development of renewable energy has increased the requirements for the energy density of lithium-ion batteries (LIBs), stimulating the exploration and research of new electrode materials. However, high energy density is often accompanied by high safety risks, and fire accidents related to LIBs are not uncommon [1,2]. Therefore, while pursuing high energy density, the safety performance of the cells must be taken into account. As the most promising new electrode material for replacing graphite anode, silicon (Si)-based anodes have received extensive attention. They have a theoretical specific capacity far higher than graphite, which meets requirements for high energy density. In addition, the abundant reserves of Si resources support the development prospects of Si-based anodes [3,4]. Si-based anodes, however, experience a significant volume effect (>300%) and produce an unstable SEI film throughout the cycle, leading to low coulombic efficiency and reversible specific capacity, which not only shortens battery life but also significantly increases the risk of thermal runaway [5,6].

The introduction of multifunctional film-forming additives is the most economical and effective method to improve the mechanical and thermal stability of electrode surfaces, which is also a current hot research topic [7]. Because solid electrolyte interface (SEI) films can adapt to the changing anode surface, the cycle performance of the battery can be significantly improved [8]. Furthermore, SEI films with excellent thermal stability can isolate the thermal reaction between Si-based anodes and electrolytes to a certain extent. This means that the electrolyte composition is essential because the chemistry and reliability

of an SEI film depend on the disintegration of the electrolyte, which in turn impacts the cycle performance and thermal stability of the batteries [9].

Additives containing functional groups such as fluoride (–F), nitrile (–C≡N), and silane have been particularly favored in the study of optimizing electrolyte formulations because these functional additives not only help to shape a uniform and strong SEI layer on the electrode, but also reduce the risk of thermal runaway batteries [10,11]. The most popular Si-based anode film-forming additives are fluoroethylene carbonate (FEC) and vinylene carbonate (VC), which can produce SEI films with high flexibility and strong ionic conductivity in an electrolyte environment [12]. Scholars used differential scanning calorimetry (DSC) to research the exothermic behavior of lithiated nano-Si electrodes in the presence of FEC and VC. The outcomes demonstrated that FEC could produce a second SEI layer on the surface of the anode, prolonging the thermal reaction time [13]. It was reported that vinyl tris(2-methoxyethoxy) silane (VTMS) was used as an additive to form a stable SEI layer on the surface of a Si/C anode, which improved the battery cycle performance [14]. 1,3,5-tris (3,3,3-trifluoropropyl) methylcyclotrisiloxane (3FO) was used as a novel additive to stabilize the interfacial structure and scavenge part of HF [15].

Although FEC is considered the most suitable silicon-based anode film-forming additive, many problems still cannot be solved. At high temperatures, FEC rapidly consumes and produces a large amount of gas, causing safety problems [8,16]. Therefore, it is necessary to find new additives to deal with the capacity fading and thermal stability of Si-based anode LIBs. A study mentioned a silane-based polymer compound (2-cyanoethyl) triethoxysilane (TCN) as a film-forming additive for SiO/C anode half-cells. TCN, as an electrolyte additive, improved the electrochemical performance of Si-based anode LIBs, which was attributed to the positive effect of nitrile-functionalized silane on SEI film formation. However, the impact of TCN on the thermal performance of the battery has not received attention [17]. As the most popular commercial Si-based anode material, SiO provides an obvious advantage by improving the energy density of the battery. The theoretical specific capacity (2615 mAh/g) of SiO is much larger than that of graphite (372 mAh/g), and its volume expansion rate (~200%) is smaller than that of monocrystalline silicon (~300%) [18]. Moreover, the SiO/C composite formed after carbon coating has higher specific capacity reversibility, so improving the battery performance under SiO-based anode is a hot issue. Charge–discharge cycling work demonstrated the better cycling performance of a battery under the action of TCN, and the subsequent cyclic voltammogram (CV) and X-ray photoelectron spectroscopy (XPS) results also revealed the formation of a better SEI layer. In addition, the thermal analysis of lithiated anodes with different electrolytes was carried out by DSC and thermogravimetric analysis (TGA). Compared with previous studies, we focused more on the safety performance of batteries under the action of additives, so we used a variety of kinetic models to assess the thermal stability of lithiated anode mixtures with different electrolytes [19–21].

2. Materials and Methods

2.1. Preparation of Electrolytes and Electrodes

The blank electrolyte (BL) was 1.0 M LiPF$_6$ in ethylene carbonate/dimethyl carbonate (EC/DMC (1:1 by volume), Sigma-Aldrich Co., St. Louis, MO, USA). The additive TCN (purity >99%, Sigma-Aldrich Co.) was directly used without purification, and 5 vol% TCN was selected as a multifunctional additive to be added to BL to obtain the modified electrolyte BL-TCN. The configuration process of the electrolyte was in an argon-filled glove box (JMS-S1X, Nanjing Jiumen Automation Technology Co., Nanjing, China), and the water and oxygen content was less than 0.1 ppm.

SiO/C composite material was selected as the active material of the Si-based anode, in which the content of SiO was 10 wt%, and the graphite content was 90 wt%. The electrode paste was prepared by mixing 90 wt% SiO/C composite, 4 wt% polymerized styrene-butadiene rubber (SBR), 3 wt% conductive agent Super-P (SP), and 3 wt% carboxymethyl cellulose (CMC) in an appropriate amount of deionized water after ball-milling

(400 r/min, 4 h). The electrode paste's components were all bought from Kejing Shenzhen Co., Shenzhen, China. After thoroughly mixing the slurry, it was evenly spread on copper foil and dried at 80 °C for 12 h. The dry electrode was cut with a diameter of 14 mm to ensure that the active substance content on the electrode was 5.95–7.51 mg/cm^2.

2.2. Electrochemical Measurements

The electrochemical test objects were CR2032 Li/SiO@C half-cells, in which the working electrode was SiO/C, the counter electrode was a Li sheet, and the separator material was a Celgard 2500 membrane. Each half-cell contained 100 μL of electrolyte, and all cell construction procedures were carried out in a glove box filled with argon. Before testing, all cells were left for 8 h to ensure that the electrolyte sufficiently penetrated the separator and electrodes. Then, using a Neware test system (CT-4008T-5V10 mA, Neware Co., Shenzhen, China), the cells were tested in a voltage window of 0.001–2.000 V. All the test objects were first cycled at 0.1 C for three cycles and then at 0.2 C for 100 cycles. Finally, cyclic voltammogram (CV) tests were conducted on the cells using an electrochemistry workstation (CHI660E, Chenhua Co., Shanghai, China) at a scanning rate of 0.001 V/s and a voltage range of 0–3 V to investigate the reversibility of the cells under various electrolyte formulations.

2.3. XPS Measurement

An XPS (Thermo Scientific K-Alpha+, Thermo Fisher Co., Waltham, MA, USA) test was carried out to determine the chemical environment of the anode surface under the action of additive TCN. The XPS test object was the anode sheet powder of the discharged battery after 15 charge–discharge cycles because the coulombic efficiency of the battery tended to be stable at this time, and the SEI film was completely formed. The pole pieces obtained after battery disassembly were cleaned with dimethyl carbonate (DMC) to remove impurities. The electrode after the battery was disassembled in the glove box was washed with dimethyl carbonate (DMC) to eliminate the remaining lithium salt and electrolyte. After that, the electrode was dried in the glove box for 12 h at room temperature.

2.4. Differential Scanning Calorimetry and Thermogravimetric Analysis

In this work, the combination of electrolyte and lithiated anode was examined by DSC (Mettler Toledo Co., Zurich, Switzerland) to study the thermal behavior of the cells during heating and evaluate the thermal stability of the batteries with BL and BL-TCN electrolytes [22,23]. The mixture of 4 mg cleaned lithiated anode powder and 5 μL electrolyte was sealed in an alumina crucible in the glove box. The material in the crucible weighed around 10 ± 0.5 mg and was heated between 30 and 350 °C at a rate of 6 °C/min [24,25].

TGA was used to test the relationship between sample mass loss and temperature change during heating [26]. The fresh and unwashed lithiated anode powder was used as the TGA test object to observe its mass loss. The test process was carried out in a nitrogen atmosphere, and the sample mass was about 10 mg. Five tests were carried out at heating rates of 1, 2, 4, 6, and 10 °C/min [27,28].

2.5. Thermokinetic Analysis

We evaluated the reaction rates between the anode powder and different electrolytes, and their thermal reaction kinetics were investigated based on TGA data at various heating rates and kinetic models. Kinetic models have been widely used as an effective tool to study the thermokinetic reactions of substances, such as the three typical non-isothermal kinetic methods that we used in this study, and the reliability of the conclusions was increased by comparing the calculation results under different models [22,27].

2.5.1. KAS Method

The Kissinger–Akahira–Sunose (KAS) model is a dynamic method approximated by the Coats–Redfern temperature integral [29,30]. The KAS model makes the calculation of activation energy (E_a) more accurate, as shown in Equation (1):

$$ln\left(\frac{\beta}{T_P^2}\right) = ln\left(\frac{A}{E_a g(\alpha)}\right) - \frac{E_a}{R \cdot T_P} \tag{1}$$

where β is the heating rate, K/min; T_p is the reaction temperature, K; α is the conversion rate; A is the pre-exponential factor; R is the ideal gas constant, $R = 8.314$ J/(mol·K); and $g(\alpha)$ is the reaction function.

2.5.2. FWO Method

The Flynn–Wall–Ozawa (FWO) method, recommended by the International Conference on Thermal Analysis and Calorimetry, is also a widely used thermokinetic model [31]. Each α value corresponds to different β values. There is a linear relationship between lnβ and $1/T$; E_a is calculated from the slope [32,33]. The kinetic model is shown in Equation (2):

$$\ln\beta = \ln\left(\frac{A E_a}{R \cdot G(\alpha)}\right) - 2.315 - 0.4567\frac{E_a}{R \cdot T} \tag{2}$$

where T is absolute temperature, K; $G(\alpha)$ is the fixed value.

2.5.3. Starink Method

The Starink model is one of the most accurate differential thermal kinetic models widely used by many researchers [20,34,35]. The model is shown in Equation (2):

$$ln\left(\frac{\beta}{T^{1.8}}\right) = C_s - 1.0037\left(\frac{E_a}{R \cdot T}\right) \tag{3}$$

where C_s is usually a constant.

3. Results and Discussion

3.1. Electrochemical Performance and Interface Properties

The batteries with various electrolyte formulations were cycled three times at 0.1 C and subsequently 100 times at 0.2 C to produce the capacity attenuation curve depicted in Figure 1, which was used to study the cycle performance of the cells. Both batteries showed fast capacity deterioration, but the capacity fading of the battery containing TCN was significantly slower than that of the BL electrolyte, showing better cycle stability. From the initial cycles, the capacity decay of the BL group began to slow after three cycles, indicating that the SEI film formed after the third charge and discharge. However, the capacity fading of the BL-TCN group began to slow after ten cycles, which showed that the building of the SEI layer in the standard electrolyte was slow and that the addition of the TCN had a favorable impact on the formation of the SEI layer. Figure 2 shows the CV test results for the first three cycles of different electrolytes, which show an enormous difference. In Figure 2b, during the first cycle of the discharge process, a reduction peak was seen at about 1.47 V, which was not seen in the blank samples, indicating that TCN may have decomposed and formed an SEI layer [7].
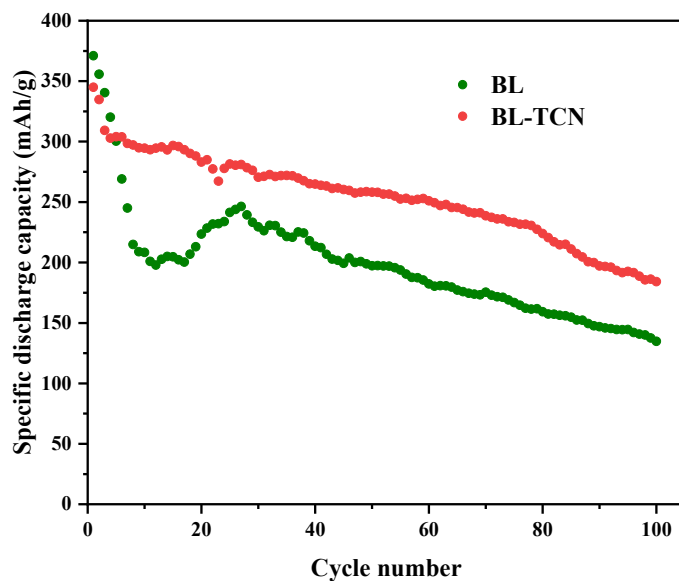
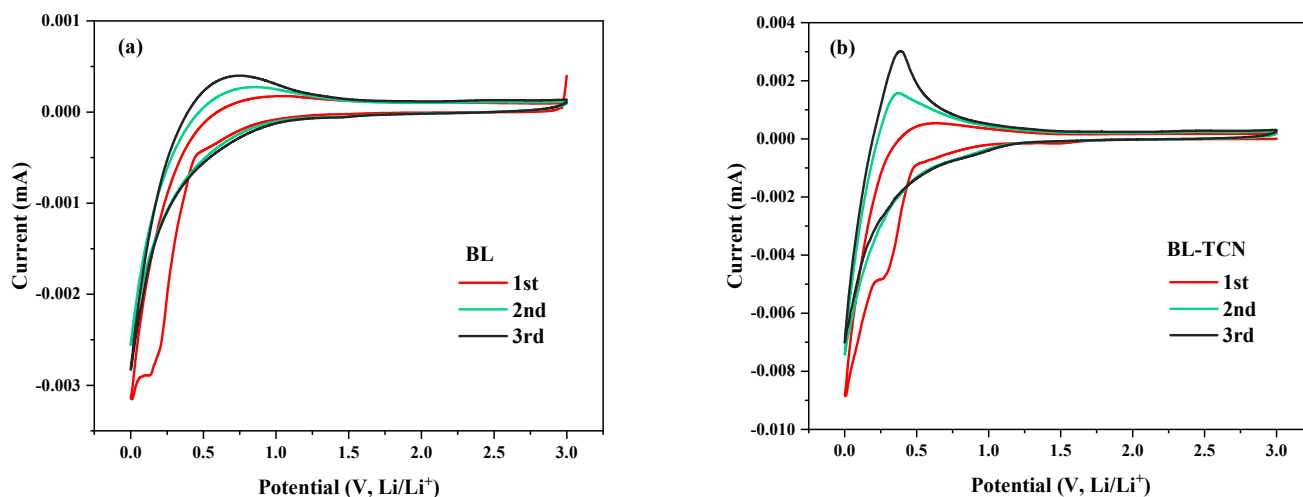**Figure 1.** Cycle performance of cells under different electrolyte formulations.

Figure 2. CV curves of Li/SiO@C half-cells at a scan rate of 0.001 V/s: (**a**) BL; (**b**) BL-TCN.

XPS was used to analyze the anode surfaces after cycling in various electrolytes, resulting in the O 1s and Li 1s spectra shown in Figure 3. For the XPS spectra of O 1s, there were three apparent peaks in the BL and BL-TCN groups, among which the peak near 531.18 eV was C=O, and the peak near 532.18 eV was C–O. Notably, the Li_2CO_3 peak at about 529.73 eV exhibited the remarkable difference between the two electrolytes. The Li_2CO_3 peak on the anode of the battery sample with the BL-TCN electrolyte after cycling was greater than that of the battery sample with the BL electrolyte, which proved that the addition of TCN was conducive to the formation of more Li_2CO_3 components on the surface of the silicon-based anode. Studies showed that the presence of more Li_2CO_3 components on the anode surface can avoid direct contact between the electrode and the electrolyte, stabilizing the electrode interface and improving the electrochemical performance of the battery [36].
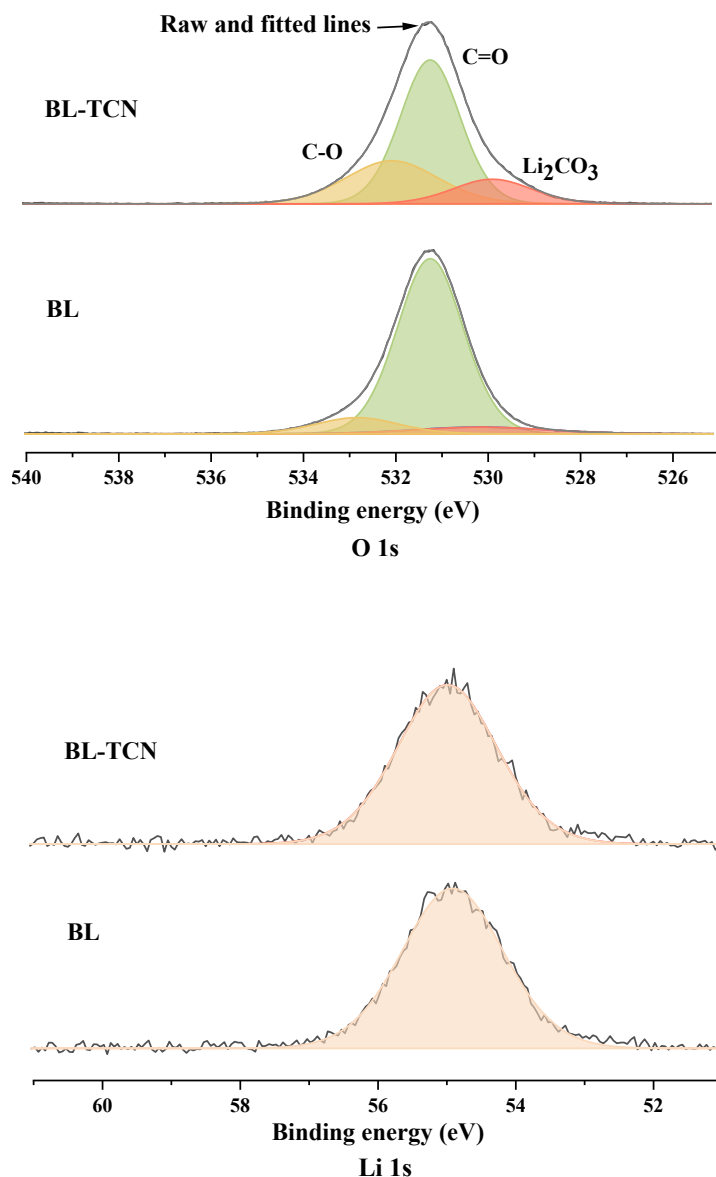
Figure 3. O 1s and Li 1s XPS spectra of anode after 15 cycles with BL and BL-TCN electrolytes.

3.2. Analysis of DSC

Given the thermal danger associated with the cohabitation of a lithiated anode and an electrolyte, the calorimetry method must be used to determine the essential thermoki-netic parameters for assessing thermal risk [10,37]. Figure 4 shows the DSC test results of the mixture of lithiated anode powder and electrolyte at a heating rate of 6 °C/min. The DSC curves of the two groups of samples showed significant exothermic peaks, and the lithiated anode with the BL electrolyte was used as the blank control group: the onset temperature (T_o) was 122.22 °C, the peak value of temperature (T_p) was 132.25 °C, and the heat of reaction (ΔH) was 240.48 J/g. When TCN was added into the electrolyte, the T_o and T_p of the mixture of anode and electrolyte increased to 127.07 °C and 133.52 °C, respectively, and the heat of reaction (ΔH) reduced to 151.71 J/g.
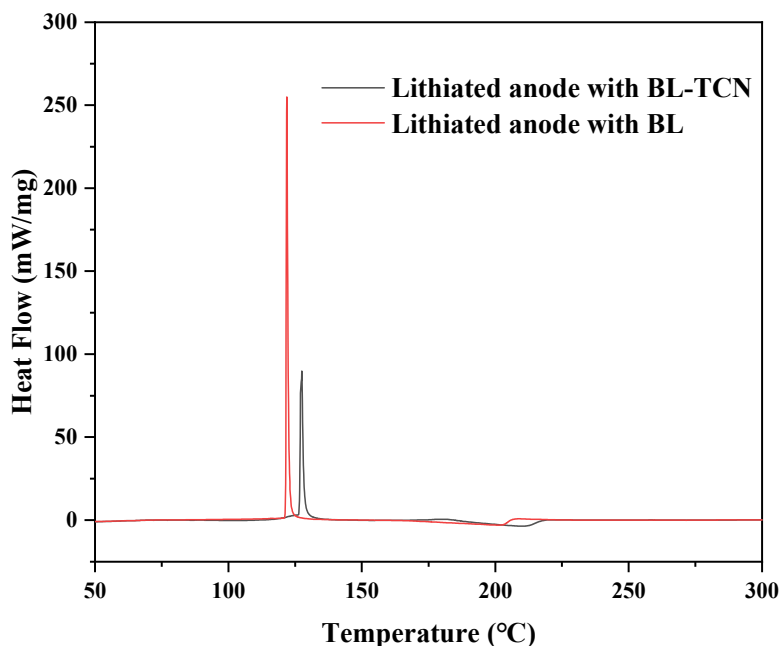
Figure 4. DSC curve of lithiated anode mixture with various electrolytes at 6 °C/min.

Table 1 presents the critical thermokinetic parameters of the admixtures of different electrolytes and anodes, which visualize the thermal hazards of lithiated anode powders in different electrolytes. For example, the BL electrolyte with a lithiated anode as a blank control sample had more severe exothermic peaks, earlier exothermic temperature, and larger ΔH. However, following the inclusion of additive TCN, the exothermic peak of the anode mixed electrolyte became smaller, and the thermal hazard was significantly reduced.

Table 1. DSC thermokinetic parameters of different samples at a heating rate of 6 °C/min.

Sample	T_o (°C)	T_p (°C)	ΔH (J/g)
Lithiated anode with BL	122.22	132.25	240.48
Lithiated anode with BL-TCN	127.07	133.52	151.71

3.3. Thermogravimetric Analysis

Figure 5 displays thermogravimetric (TG) and differential thermogravimetry (DTG) data of the lithiated anode with different electrolytes at a heating rate of 6 °C/min. The outcomes demonstrated that the samples' mass loss could be roughly divided into three parts. The first stage was the part where the temperature was lower than 90.31 °C. The main reason for mass loss during this period was the volatilization of electrolyte solvent molecules, so the mass loss rates of the two samples were the same. The second stage was a temperature range between 90.31 and 128.83 °C, where the sample mass loss rate accelerated, which may have been due to the decomposition of the electrolyte. The mass loss rate of samples containing TCN was slower, which might have occurred because TCN could impede the breakdown of the electrolyte at higher temperature. The mass loss of the third stage was between 128.83 and 138.62 °C, and the mass loss rate of the sample was the fastest at this stage, which could be attributed to the vigorous reaction between Li in the anode and the electrolyte components.
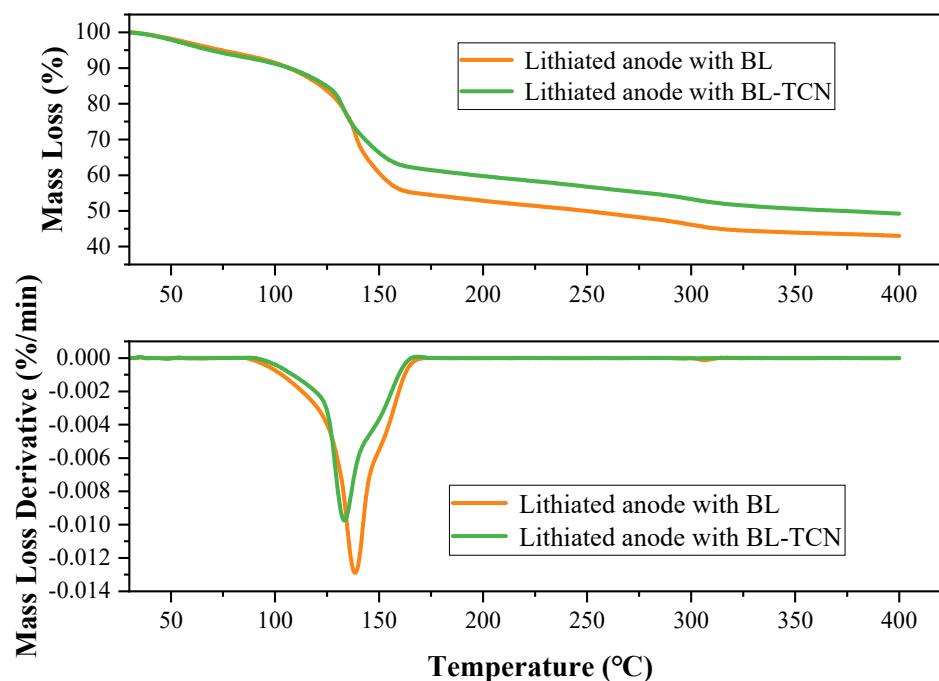
Figure 5. TG-DTG curves of lithiated anode with different electrolytes at a rate of 6 °C/min.

The mass loss of the sample without the additive was 56.93%, while the mass loss of the sample with the additive TCN was decreased to 49.98% when comparing the two sets of data with different electrolytes. The reaction of the lithiated anode with the BL-TCN electrolyte was slower and the reaction time was shorter, particularly in the third stage of mass loss. The TG results showed that additive TCN positively inhibited the exothermic reaction between the lithiated anode and electrolyte, which was consistent with the DSC results.

Figure 6 shows the difference in the TG-DTG curves under various heating rates. As β increased, the initial temperature of the reaction of the lithiated anode with the electrolyte also increased. For example, when $\beta = 1$ °C/min, the sample started an exothermic reaction at 60.95 °C and ended at 137.15 °C; the reaction rate reached its maximum at 110.12 °C; when $\beta = 10$ °C/min, the starting temperature was 87.16 °C, and the end temperature was 173.66 °C; the reaction rate reached its maximum at 138.21 °C. The TG-DTG curves showed that as β increased, the thermal reaction of the lithiated anode with the electrolyte was delayed and the thermal reaction rate slowed down. Figure 7 displays the differences in the TG-DTG curves of the BL electrolyte without TCN addition at various heating rates. As β increased, the initial temperature of the reaction of the lithiated anode with the BL electrolyte also increased, which is consistent with the trend in the TG-DTG curve for the BL-TCN electrolyte. However, compared with the anode powder containing the BL-TCN electrolyte, the mixture of BL electrolyte and anode powder showed greater mass loss and a faster mass loss rate at the same heating rate, which further confirmed the positive effect of the TCN additive on thermal stability.

3.4. Thermokinetic Analysis

Calculating E_a using thermokinetic models is a reliable way to assess the safety of substances. An equal approach was used to calculate the thermokinetic parameters of the anode and electrolyte under different thermokinetic models (KAS, Starink, and FWO) based on the thermokinetic data from TGA. Comparing the E_a values calculated using various methodologies improved the reliability of the findings [38]. Three different sets of fitting results are obtained using kinetic models. Each set of fitting results contain multiple fitted lines under various α, and E_a can be calculated according to the slope of the fitted

lines. For example, in the KAS model, there is a linear relationship between $\ln(\beta/T_\alpha^2)$ and $1/T$, and the slope of their fitting line determines the E_a value.
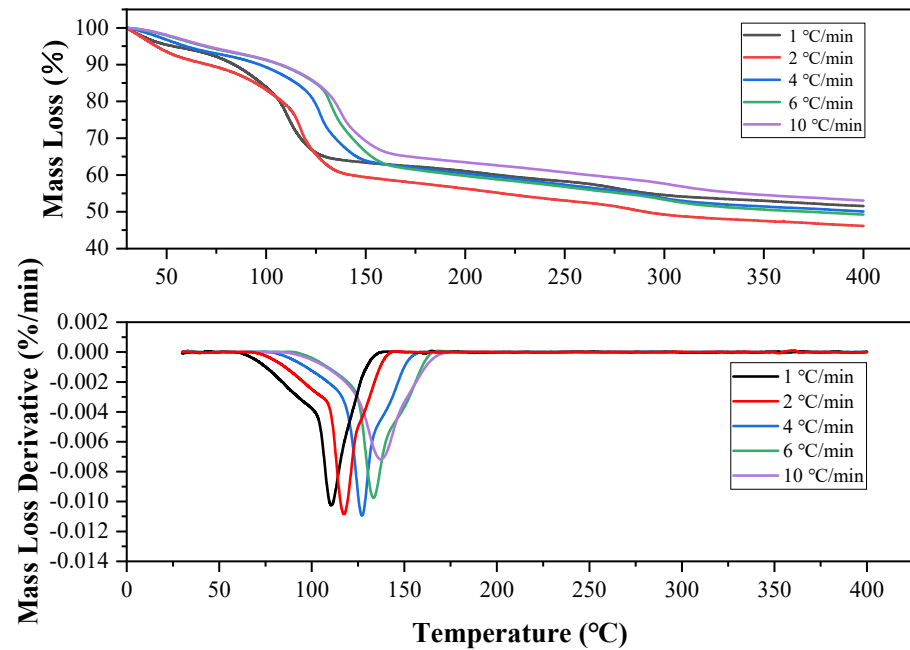

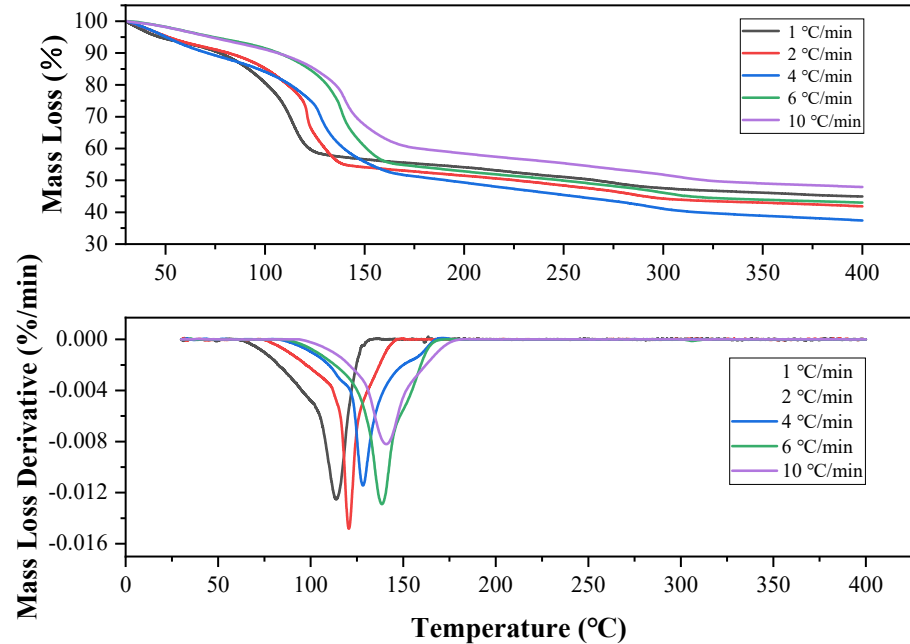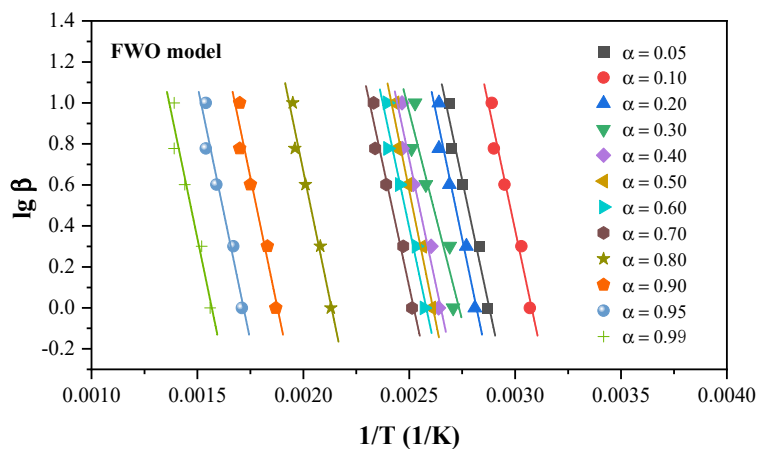**Figure 6.** TG-DTG curve of lithiated anode with BL-TCN electrolyte at different β.


Figure 7. TG-DTG curve of lithiated anode with BL electrolyte at different β.

The E_a values of mixtures of different electrolytes and lithiated anode powders were calculated at five heating rates (β = 1.0, 2.0, 4.0, 6.0, and 10 °C/min), and 12 various α values were used for differential isoconversional analysis. Figure 8 shows the fitting results for different α values under the three kinetic models. In addition, the fitting results calculated by the KAS model are given in Figure 8, and the trends in the fitted lines for different α values tended to be consistent. This phenomenon also existed in the FWO and Starink
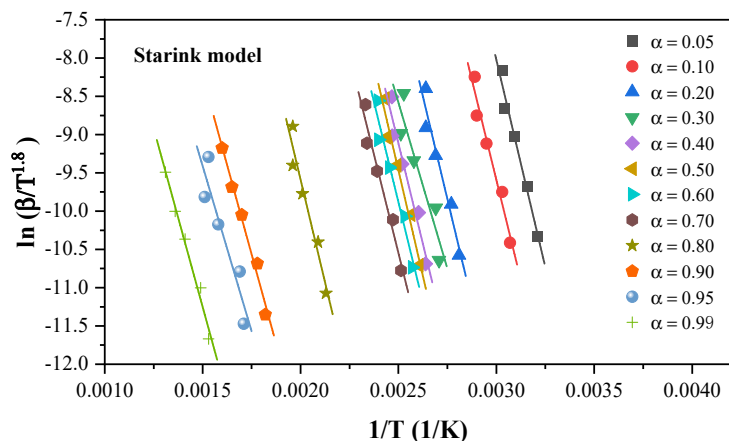
models, which confirmed the applicability of these models and the reasonableness of the calculated results.

(**a**)
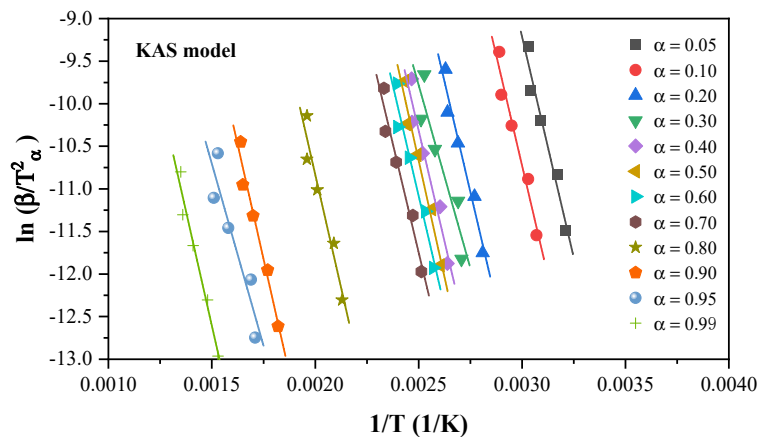
(**b**)

(**c**)

Figure 8. Differential isoconversional analysis of lithiated anode with BL-TCN using three methods at 1, 2, 4, 6, and 10 °C/min in TG experiments: (**a**) FWO model; (**b**) KAS model; (**c**) Starink model.

Table 2 lists the E_a and coefficient of determination (R^2) values of the lithiated anode with BL-TCN calculated by the various methods. The E_a values corresponding to the 12 α values in each model showed slight differences, and the corresponding R^2 values were all above 0.90 and close to 1.00, which further confirmed the reliability of the results. All the E_a values corresponding to the 12 α values were averaged to obtain the final outcome of the E_a value in each model. As shown in Table 2, the E_a values calculated by the three kinetic models were 90.88, 92.15, and 90.94 kJ/mol, respectively, and the corresponding R^2 values were 0.9487, 0.9469, and 0.9506, respectively.

Table 2. E_a and R^2 of the lithiated anode with BL-TCN in various models.

α	E_a (kJ/mol)			R^2		
	KAS	FWO	Starink	KAS	FWO	Starink
0.05	91.93	91.56	91.69	0.9595	0.9654	0.9698
0.10	87.59	92.36	91.65	0.9485	0.9572	0.9602
0.20	89.30	91.37	90.92	0.9664	0.9368	0.9430
0.30	90.70	89.95	89.22	0.9084	0.9070	0.9004
0.40	90.69	92.12	90.96	0.9392	0.9683	0.9400
0.50	94.59	93.30	93.52	0.9637	0.9518	0.9643
0.60	89.47	91.18	89.84	0.9445	0.9621	0.9453
0.70	86.69	92.15	91.45	0.9561	0.9735	0.9568
0.80	89.98	91.60	91.05	0.9422	0.9496	0.9428
0.90	92.65	93.71	89.59	0.9694	0.9542	0.9832
0.95	94.52	92.18	90.89	0.9165	0.9238	0.9186
0.99	92.42	94.29	90.45	0.9694	0.9128	0.9832
Average	90.88	92.15	90.94	0.9487	0.9469	0.9506

Table 3 shows the comparison results of the E_a values calculated by the two samples under different kinetic models. For the samples of the lithiated anode with BL electrolyte, the average value of E_a calculated by the three models was 68.46 kJ/mol, which was lower than the E_a value of the material after the addition of additive TCN. The E_a is the energy needed for molecules to change from normal to active states prone to chemical reactions [20]. Therefore, the higher the E_a is, the higher the difficulty of material reaction is, and the safer the material. The addition of TCN increased the E_a value of the lithiated anode powder mixed electrolyte from 68.46 kJ/mol to 91.32 kJ/mol, proving that the additive TCN had an enormously beneficial result in suppressing the exothermic reaction between the lithiated anode and the electrolyte, which was consistent with the analysis results of DSC and TG.

Table 3. E_a and R^2 of lithiated anode with various electrolytes in three thermokinetic models.

	Lithiated Anode with BL		Lithiated Anode with BL-TCN	
	E_a (kJ/mol)	R^2	E_a (kJ/mol)	R^2
KAS	68.47	0.9558	90.88	0.9487
FWO	69.51	0.9637	92.15	0.9469
Starink	67.39	0.9426	90.94	0.9506
Average	68.46	0.9540	91.32	0.9487

4. Conclusions

In this process, a silane-based polymer compound, TCN, was added to a commercial electrolyte at a volume ratio of 5%, and satisfactory results were obtained. During long-term charge–discharge cycles, the cells containing TCN exhibited better cycling stability, mainly attributed to the fact that TCN contributed to forming a more stable SEI film. In addition, the XPS results showed that the SEI film formed in the electrolyte containing TCN had more Li_2CO_3 components, which enhanced the SEI film's mechanical stability.

The DSC results showed that the addition of TCN considerably inhibited the exothermic reaction between the lithiated anode and electrolyte, which mainly manifested in the

decrease in heat release and the increase in reaction starting temperature; namely, ΔH decreased from 250.48 to 151.71 J/g, and T_o increased from 122.22 to 127.07 °C. The TG results showed that the samples containing TCN had a minor mass loss and a slower mass loss rate, indicating the positive effect of TCN on inhibiting the reaction between the electrolyte and anode, which was mutually confirmed with the DSC results. Furthermore, the addition of TCN increased the E_a value of the lithiated anode–electrolyte mixture from 68.46 to 91.32 kJ/mol according to results of thermokinetic analysis, further confirming the contribution of TCN to the safety performance of Si-based anode LIBs. This study provides a new feasible idea for developing intrinsically safe, high-energy-density batteries.

Author Contributions: Conceptualization, C.-Z.Z.; data processing, L.-J.X.; software, Y.T.; language polish, Y.L.; supervision, J.-C.J.; methodology, A.-C.H. All authors have read and agreed to the published version of the manuscript.

Institutional Review Board Statement: Not applicable.

Informed Consent Statement: Not applicable.

Conflicts of Interest: The authors declare no conflict of interest.

References

1. Yuan, M.; Liu, K. Rational design on separators and liquid electrolytes for safer lithium-ion batteries. *J. Energy Chem.* **2020**, *43*, 58–70. [CrossRef]
2. Wu, Z.H.; Huang, A.C.; Tang, Y.; Yang, Y.P.; Liu, Y.C.; Li, Z.P.; Zhou, H.L.; Huang, C.F.; Xing, Z.X.; Shu, C.M.; et al. Thermal Effect and Mechanism Analysis of Flame-Retardant Modified Polymer Electrolyte for Lithium-Ion Battery. *Polymers* **2021**, *13*, 1675. [CrossRef] [PubMed]
3. Jin, Y.; Zhu, B.; Lu, Z.; Liu, N.; Zhu, J. Challenges and Recent Progress in the Development of Si Anodes for Lithium-Ion Battery. *Adv. Energy Mater.* **2017**, *7*, 1700715. [CrossRef]
4. Liang, B.; Liu, Y.; Xu, Y. Silicon-based materials as high capacity anodes for next generation lithium ion batteries. *J. Power Sources* **2014**, *267*, 469–490. [CrossRef]
5. Sun, S.; He, D.; Li, P.; Liu, Y.; Wan, Q.; Tan, Q.; Liu, Z.; An, F.; Gong, G.; Qu, X. Improved adhesion of cross-linked binder and SiO_2-coating enhances structural and cyclic stability of silicon electrodes for lithium-ion batteries. *J. Power Sources* **2020**, *454*, 227907. [CrossRef]
6. Wang, D.; Gao, M.; Pan, H.; Liu, Y.; Wang, J.; Li, S.; Ge, H. Enhanced cycle stability of micro-sized Si/C anode material with low carbon content fabricated via spray drying and in situ carbonization. *J. Alloy. Compd.* **2014**, *604*, 130–136. [CrossRef]
7. Shen, J.; Chen, H.; Yu, L.; Huang, D.; Luo, Z. 4, 5-difluoro-1, 3-dioxolan-2-one as an film forming additive on $LiNi_{0.8}Co_{0.15}Al_{0.05}O_2$/$SiO@C$ full cells. *J. Electroanal. Chem.* **2019**, *834*, 1–7. [CrossRef]
8. Zhang, C.-Z.; Jiang, J.-C.; Huang, A.-C.; Tang, Y.; Xie, L.-J.; Zhai, J.; Xing, Z.-X. A novel multifunctional additive strategy improves the cycling stability and thermal stability of SiO/C anode Li-ion batteries. *Process. Saf. Environ. Prot.* **2022**, *164*, 555–565. [CrossRef]
9. Nigl, T.; Baldauf, M.; Hohenberger, M.; Pomberger, R. Lithium-Ion Batteries as Ignition Sources in Waste Treatment Processes—A Semi-Quantitate Risk Analysis and Assessment of Battery-Caused Waste Fires. *Processes* **2020**, *9*, 49. [CrossRef]
10. Profatilova, I.A.; Stock, C.; Schmitz, A.; Passerini, S.; Winter, M. Enhanced thermal stability of a lithiated nano-silicon electrode by fluoroethylene carbonate and vinylene carbonate. *J. Power Sources.* **2013**, *222*, 140–149. [CrossRef]
11. Yang, Y.-P.; Jiang, J.-C.; Huang, A.-C.; Tang, Y.; Liu, Y.-C.; Xie, L.-J.; Zhang, C.-Z.; Wu, Z.-h.; Xing, Z.-X.; Yu, F. 3-(Trifluoromethyl)benzoylacetonitrile: A multi-functional safe electrolyte additive for $LiNi_{0.8}Co_{0.1}Mn_{0.1}O_2$ cathode of high voltage lithium-ion battery. *Process. Saf. Environ. Prot.* **2022**, *160*, 80–90. [CrossRef]
12. Profatilova, I.A.; Kim, S.-S.; Choi, N.-S. Enhanced thermal properties of the solid electrolyte interphase formed on graphite in an electrolyte with fluoroethylene carbonate. *Electrochim. Acta.* **2009**, *54*, 4445–4450. [CrossRef]
13. Zhang, S.S. Electrochemical study of the formation of a solid electrolyte interface on graphite in a LiBC2O4F2-based electrolyte. *J. Power Sources* **2007**, *163*, 713–718. [CrossRef]
14. Wang, J.; Zhang, L.; Zhang, H. Effects of electrolyte additive on the electrochemical performance of Si/C anode for lithium-ion batteries. *Ionics* **2018**, *24*, 3691–3698. [CrossRef]
15. Xu, N.; Sun, Y.; Shi, J.; Chen, J.; Liu, G.; Zhou, K.; He, H.; Zhu, J.; Zhang, Z.; Yang, Y. Fluorinated cyclic siloxane additives for high energy density Li-ion batteries with high nickel cathodes and silicon–carbon anodes. *J. Power Sources* **2021**, *511*, 230437. [CrossRef]

16. Schiele, A.; Breitung, B.; Hatsukade, T.; Berkes, B.B.; Hartmann, P.; Janek, J.; Brezesinski, T. The Critical Role of Fluoroethylene Carbonate in the Gassing of Silicon Anodes for Lithium-Ion Batteries. *ACS Energy Lett.* **2017**, *2*, 2228–2233. [CrossRef]

17. Aupperle, F.; Eshetu, G.G.; Eberman, K.W.; Xioa, A.; Bridel, J.-S.; Figgemeier, E. Realizing a high-performance LiNi0.6Mn0.2Co0.2O2/silicon–graphite full lithium ion battery cell via a designer electrolyte additive. *J. Mater. Chem. A* **2020**, *8*, 19573–19587. [CrossRef]

18. Yang, Y.; Yang, Z.; Xu, Y.; Li, Z.; Yao, N.; Wang, J.; Feng, Z.; Wang, K.; Xie, J.; Zhao, H. Synergistic effect of vinylene carbonate (VC) and LiNO3 as functional additives on interphase modulation for high performance SiO anodes. *J. Power Sources* **2021**, *514*, 230595. [CrossRef]

19. Xie, L.-J.; Jiang, J.-C.; Huang, A.-C.; Tang, Y.; Liu, Y.-C.; Zhou, H.-L.; Xing, Z.-X. Calorimetric Evaluation of Thermal Stability of Organic Liquid Hydrogen Storage Materials and Metal Oxide Additives. *Energies* **2022**, *15*, 2236. [CrossRef]

20. Huang, A.-C.; Li, Z.-P.; Liu, Y.-C.; Tang, Y.; Huang, C.-F.; Shu, C.-M.; Xing, Z.-X.; Jiang, J.-C. Essential hazard and process safety assessment of para-toluene sulfonic acid through calorimetry and advanced thermokinetics. *J. Loss Prev. Process. Ind.* **2021**, *72*, 104558. [CrossRef]

21. Taco-Vasquez, S.; Ron, C.A.; Murillo, H.A.; Chico, A.; Arauz, P.G. Thermochemical Analysis of a Packed-Bed Reactor Using Finite Elements with FlexPDE and COMSOL Multiphysics. *Processes* **2022**, *10*, 1144. [CrossRef]

22. Huang, A.-C.; Liao, F.-C.; Huang, C.-F.; Tang, Y.; Zhang, Y.; Shu, C.-M.; Xing, Z.-X.; Jiang, J.-C.; Hsieh, W.-Y. Calorimetric approach to establishing thermokinetics for cosmeceutical benzoyl peroxides containing metal ions. *J. Therm. Anal. Calorim.* **2021**, *144*, 373–382. [CrossRef]

23. Li, Z.P.; Jiang, J.C.; Huang, A.C.; Tang, Y.; Miao, C.F.; Zhai, J.; Huang, C.F.; Xing, Z.X.; Shu, C.M. Thermal hazard evaluation on spontaneous combustion characteristics of nitrocellulose solution under different atmospheric conditions. *Sci. Rep.* **2021**, *11*, 24053. [CrossRef] [PubMed]

24. Silva, J.B.; Almeida, J.S.; Barbosa, R.V.; Fernandes, G.J.T.; Coriolano, A.C.F.; Fernandes, V.J.; Araujo, A.S. Thermal Oxidative Stability of Biodiesel/Petrodiesel Blends by Pressurized Differential Scanning Calorimetry and Its Calculated Cetane Index. *Processes* **2021**, *9*, 174. [CrossRef]

25. Merighi, S.; Mazzocchetti, L.; Benelli, T.; Giorgini, L. Evaluation of Novel Bio-Based Amino Curing Agent Systems for Epoxy Resins: Effect of Tryptophan and Guanine. *Processes* **2020**, *9*, 42. [CrossRef]

26. Yao, C.; Liu, Y.-C.; Wu, J.; Tang, Y.; Zhai, J.; Shu, C.-M.; Jiang, J.-C.; Xing, Z.-X.; Huang, C.-F.; Huang, A.-C. Thermal Stability Determination of Propylene Glycol Sodium Alginate and Ammonium Sulfate with Calorimetry Technology. *Processes* **2022**, *10*, 1177. [CrossRef]

27. Zhang, M.-L.; Dong, X.-L.; Tang, Y.; Huang, A.-C.; Chen, F.; Kang, Q.-C.; Shu, Z.-J.; Xing, Z.-X. Experimental investigations of extinguishing sodium pool fires using modified expandable graphite powders. *Case Stud. Therm. Eng.* **2022**, *32*, 101911. [CrossRef]

28. Yin, X.-Y.; Liu, T.; Liu, Y.-C.; Tang, Y.; Huang, A.-C.; Dong, X.-L.; Liu, Y.-J. Feasibility Study of Fine Water Mist Applied to Cold Storage Fire Protection. *Processes* **2022**, *10*, 1533. [CrossRef]

29. Chen, F.; Dong, X.-L.; Tang, Y.; Huang, A.-C.; Zhang, M.-L.; Kang, Q.-C.; Shu, Z.-J.; Xing, Z.-X. Thermal Characteristic Analysis of Sodium in Diluted Oxygen via Thermogravimetric Approach. *Processes* **2022**, *10*, 704. [CrossRef]

30. Huang, A.-C.; Huang, C.-F.; Tang, Y.; Xing, Z.-X.; Jiang, J.-C. Evaluation of multiple reactions in dilute benzoyl peroxide concentrations with additives using calorimetric technology. *J. Loss Prev. Process. Ind.* **2021**, *69*, 104373. [CrossRef]

31. Vyazovkin, S.; Sbirrazzuoli, N. Isoconversional Kinetic Analysis of Thermally Stimulated Processes in Polymers. *Macromol. Rapid Commun.* **2006**, *27*, 1515–1532. [CrossRef]

32. Yang, N.; Jiang, J.-C.; Huang, A.-C.; Tang, Y.; Li, Z.-P.; Cui, J.-W.; Shu, C.-M.; Xing, Z.-X. Thermokinetic model-based experimental and numerical investigation of the thermal hazards of nitrification waste. *J. Loss Prev. Process. Ind.* **2022**, *79*, 104836. [CrossRef]

33. Liu, Y.-C.; Huang, A.-C.; Tang, Y.; Huang, C.-F.; Shen, Q.; Shu, C.-M.; Xing, Z.-X.; Jiang, J.-C. Thermokinetic analysis of the stability of acetic anhydride hydrolysis in isothermal calorimetry techniques. *J. Therm. Anal. Calorim.* **2021**, *147*, 7865–7873. [CrossRef]

34. Liu, Y.-C.; Huang, A.-C.; Tang, Y.; Ma, X.-M.; Yang, Y.-P.; Wu, Z.-H.; Shu, C.-M.; Xing, Z.-X.; Jiang, J.-C. Thermokinetic model establishment and numerical simulation of 2,4,6-trinitrophenol based on eco-friendly synthesis method. *J. Energetic Mater.* **2021**, 1–20. [CrossRef]

35. Yepes, C.; Estévez, J.; Arroyo, M.; Ladero, M. Immobilization of an Industrial β-Glucosidase from *Aspergillus fumigatus* and Its Use for Cellobiose Hydrolysis. *Processes* **2022**, *10*, 1225. [CrossRef]

36. Verma, P.; Maire, P.; Novák, P. A review of the features and analyses of the solid electrolyte interphase in Li-ion batteries. *Electrochim. Acta.* **2010**, *55*, 6332–6341. [CrossRef]

37. Chang, T.; Hsueh, K.-H.; Liu, C.-C.; Cao, C.-R.; Shu, C.-M. A Method to Derive the Characteristic and Kinetic Parameters of 1,1-Bis(tert-butylperoxy)cyclohexane from DSC Measurements. *Processes* **2022**, *10*, 1026. [CrossRef]

38. Liu, Y.-C.; Jiang, J.-C.; Huang, A.-C.; Tang, Y.; Yang, Y.-P.; Zhou, H.-L.; Zhai, J.; Xing, Z.-X.; Huang, C.-F.; Shu, C.-M. Hazard assessment of the thermal stability of nitrification by-products by using an advanced kinetic model. *Process. Saf. Environ. Prot.* **2022**, *160*, 91–101. [CrossRef]